Correction

NEUROSCIENCE

Correction for "Activity-dependent bulk endocytosis proteome reveals a key presynaptic role for the monomeric GTPase Rab11," by A. C. Kokotos, J. Peltier, E. C. Davenport, M. Trost, and M. A. Cousin, which was first published October 9, 2018; 10.1073/pnas.1809189115 (*Proc Natl Acad Sci USA* 115:E10177–E10186).

The authors note that Fig. 1 and Fig. 2 appeared incorrectly. The corrected figures and their legends appear below. The authors also note that on page E10178, right column, first full paragraph, lines 4–9, the following text appeared incorrectly: "Cluster analysis using DAVID annotations revealed the top two clusters enriched were identical to those identified with the Nycodenz fractionation protocol, synapse and cell adhesion. In addition, other enriched clusters were cytoskeleton and GTP binding (Fig. 2*E* and Dataset S6)." It should instead appear as: "Cluster analysis using DAVID annotations revealed the top three clusters enriched were almost identical to those identified with the Nycodenz fractionation protocol, cell adhesion, cytoskeleton, and synapse (Fig. 2*E* and Dataset S6)." These errors do not affect the conclusions of the article.

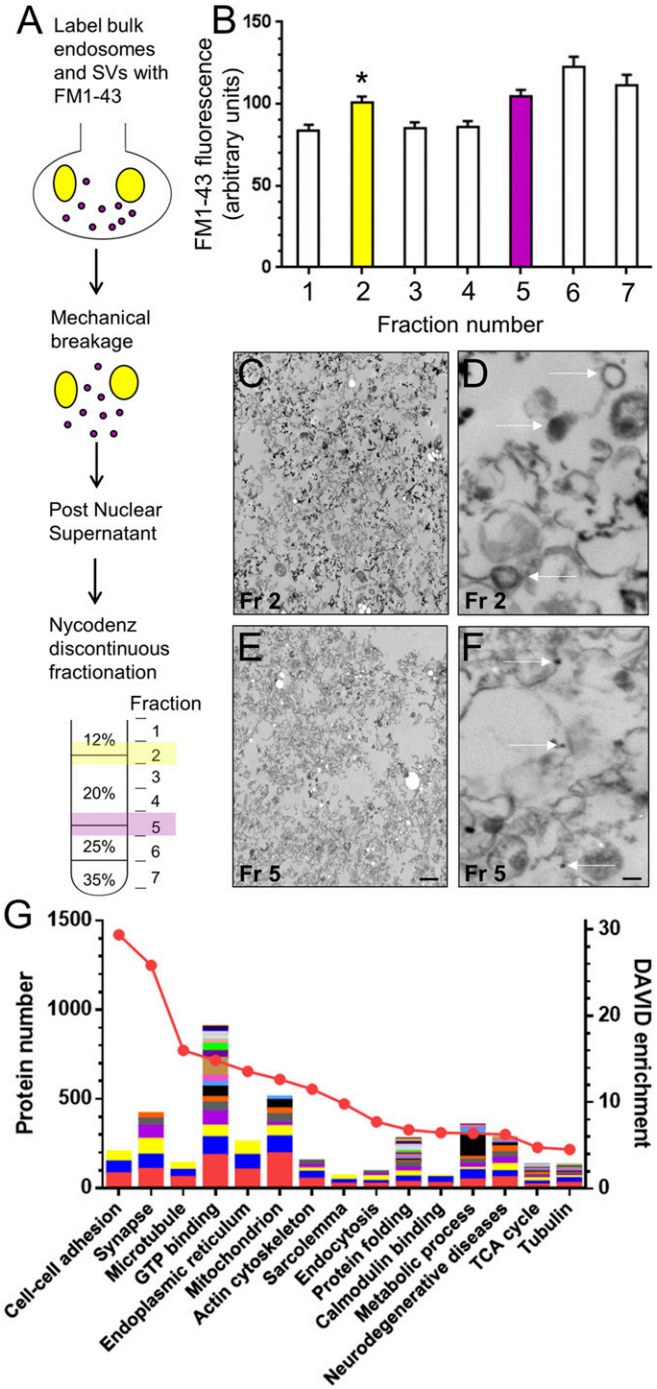

Fig. 1. Bulk endosome proteome generated via Nycodenz fractionation. (*A*) Protocol for enrichment of bulk endosomes. Primary cultures of cerebellar granule neurons were stimulated using 50 mM KCl for 2 min in the presence of 10 μM FM1-43. Cells were washed thoroughly, harvested, and lysed mechanically using a ball-bearing cell cracker. The postnuclear supernatant was generated and submitted to subcellular fractionation using discontinuous Nycodenz gradients (12, 20, 25, and 35%). (*B*) Seven fractions were obtained (1–7) and their fluorescence was quantified after normalization to the PNS fraction (normalized to 900 arbitrary units). Fraction 2 (yellow) and fraction 5 (purple) are highlighted since they contain bulk endosomes and SVs, respectively (all $n = 6 \pm$ SEM, $^*P < 0.05$, one-way ANOVA fractions 1–4). (*C*–*F*) An identical protocol was performed to load 10 mg/mL HRP into bulk endosomes and SVs. After conversion of HRP to an electron-dense product, fractions 2 (Fr 2) and 5 (Fr 5) were visualized by transmission electron microscopy. Low- (*C* and *E*) and high- (*D* and *F*) magnification images are displayed. [Scale bars, 2 μm (*C* and *E*) and 200 nm (*D* and *F*).] Arrows indicate HRP-labeled structures in *D* and *F*. (*G*) Fraction 2 was subjected to LC-MS/MS analysis and the results were processed using DAVID functional annotation clustering analysis. The top 15 enriched clusters are displayed in descending order of their DAVID enrichment score on the right *y* axis. The number of proteins in each DAVID cluster is presented on the left *y* axis. Subclusters are represented as different colors. It should be noted that proteins can be represented multiple times both within and between DAVID clusters and subclusters, meaning the protein number is not a representation of the independent number of proteins per cluster.

CORRECTION

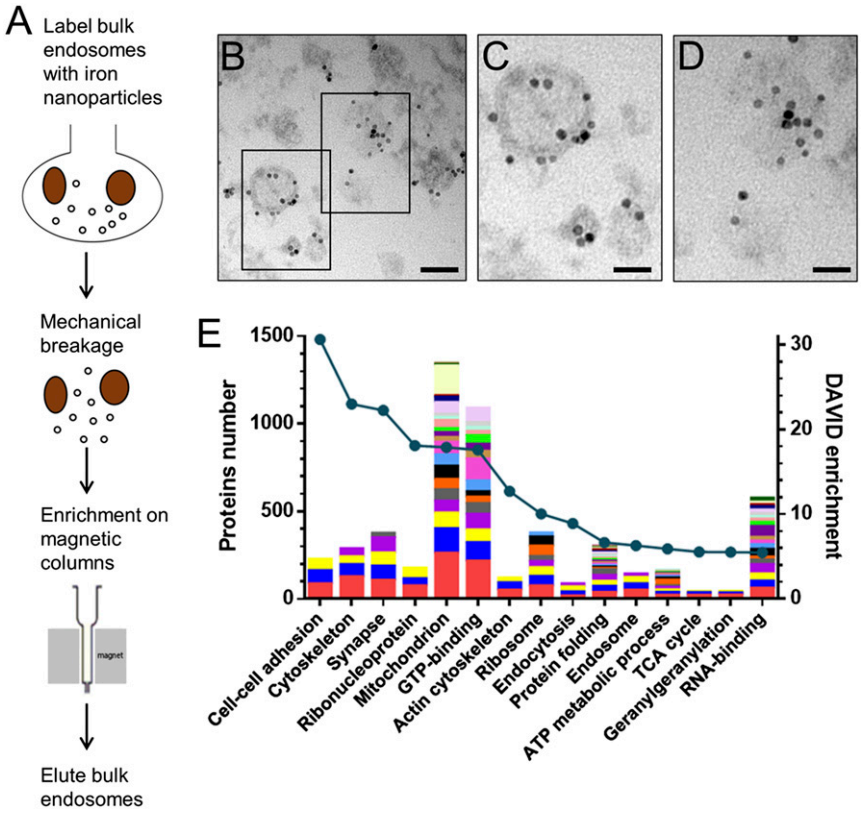

Fig. 2. Bulk endosome proteome generated via iron nanoparticle isolation. (*A*) Protocol for enrichment of bulk endosomes. Primary cultures of CGNs were stimulated using 50 mM KCl for 2 min in the presence of 1 mg/mL 10-nm iron nanoparticles. Cells were washed thoroughly, harvested, and lysed mechanically using a ball-bearing cell cracker. The postnuclear supernatant was generated and applied to magnetic columns. Retained bulk endosomes were eluted by removal from the magnet and processed for either electron microscopy or mass spectrometry analysis. (*B–D*) Representative images of the eluted bulk endosome fraction at either low- (*B*) or high- (*C* and *D*) magnification are displayed. [Scale bars, 250 nm (*B*) and 100 nm (*C* and *D*).] (*E*) Eluted bulk endosomes were subjected to LC-MS/MS analysis and the results were processed using DAVID functional annotation clustering analysis. The top 15 enriched clusters are displayed in descending order of their DAVID enrichment score on the right *y* axis. The number of proteins in each DAVID cluster is presented on the left *y* axis.

Published online January 28, 2019.

www.pnas.org/cgi/doi/10.1073/pnas.1900100116

Activity-dependent bulk endocytosis proteome reveals a key presynaptic role for the monomeric GTPase Rab11

A. C. Kokotos[a,b,c], J. Peltier[d], E. C. Davenport[a,b,c], M. Trost[d], and M. A. Cousin[a,b,c,1]

[a]Centre for Discovery Brain Sciences, University of Edinburgh, Edinburgh EH8 9XD, Scotland, United Kingdom; [b]Muir Maxwell Epilepsy Centre, University of Edinburgh, Edinburgh EH8 9XD, Scotland, United Kingdom; [c]Simons Initiative for the Developing Brain, University of Edinburgh, Edinburgh EH8 9XD, Scotland, United Kingdom; and [d]Institute for Cell and Molecular Biosciences, Faculty of Medical Sciences, Newcastle University, Newcastle upon Tyne NE2 4HH, United Kingdom

Edited by Richard L. Huganir, The Johns Hopkins University School of Medicine, Baltimore, MD, and approved September 13, 2018 (received for review May 30, 2018)

Activity-dependent bulk endocytosis (ADBE) is the dominant mode of synaptic vesicle endocytosis during high-frequency stimulation, suggesting it should play key roles in neurotransmission during periods of intense neuronal activity. However, efforts in elucidating the physiological role of ADBE have been hampered by the lack of identified molecules which are unique to this endocytosis mode. To address this, we performed proteomic analysis on purified bulk endosomes, which are a key organelle in ADBE. Bulk endosomes were enriched via two independent approaches, a classical subcellular fractionation method and isolation via magnetic nanoparticles. There was a 77% overlap in proteins identified via the two protocols, and these molecules formed the ADBE core proteome. Bioinformatic analysis revealed a strong enrichment in cell adhesion and cytoskeletal and signaling molecules, in addition to expected synaptic and trafficking proteins. Network analysis identified Rab GTPases as a central hub within the ADBE proteome. Subsequent investigation of a subset of these Rabs revealed that Rab11 both facilitated ADBE and accelerated clathrin-mediated endocytosis. These findings suggest that the ADBE proteome will provide a rich resource for the future study of presynaptic function, and identify Rab11 as a regulator of presynaptic function.

endocytosis | neuron | presynapse | vesicle | Rab11

Maintenance of neurotransmission across a range of different patterns of neuronal activity is critical for normal brain function. Activity-dependent synaptic vesicle (SV) fusion is essential for neurotransmitter release; however, the conservation of a pool of release-ready SVs is equally important for sustaining this process. There are at least three independent SV endocytosis modes that perform this role (1, 2). The first is clathrin-mediated endocytosis (CME), which is the dominant SV endocytosis mode during low levels of neuronal activity (3). However, during extremely mild neuronal activity, ultrafast endocytosis (UFE) is the dominant endocytosis mode. UFE forms large vesicles from a subcellular region directly adjacent to the presynaptic active zone, with SVs shed from synaptic endosomes within 2 to 3 s (4, 5). During elevated neuronal activity both CME and UFE saturate (3, 6, 7). To ameliorate this outcome, activity-dependent bulk endocytosis (ADBE) is triggered (7). ADBE is the dominant mode of SV endocytosis during elevated neuronal activity and generates large plasma membrane invaginations to form bulk endosomes from which functional SVs are generated (8).

The predominant role of ADBE during high-frequency stimulation suggests that it should perform key modulatory roles in physiological events triggered via elevated neuronal activity. In support, previous studies have hinted that ADBE may limit neurotransmission during trains of high-frequency stimulation (9–11). However, the process of defining the physiological role of ADBE has been hindered by the lack of identified molecules that are both essential and specific to this endocytosis mode. To address this key unmet need, we performed proteomic analysis on a specific ADBE organelle, the bulk endosome. Two independent protocols were employed to enrich bulk endosomes, which were then subjected to mass spectrometry analysis to identify the ADBE proteome. Interestingly, network analysis revealed that Rab GTPases formed a key functional hub within the ADBE proteome. Rab proteins are essential regulators of cellular trafficking and transport (12, 13), operating as "molecular switches" by virtue of their GTP- or GDP-bound state. We have therefore identified a key role for Rab11 in facilitating both ADBE and CME by exploiting information from the ADBE proteome and optical assays of SV recycling.

Results

The Molecular Inventory of Bulk Endosomes Enriched via Biochemical Fractionation. To identify molecules required for ADBE, we employed two parallel protocols to enrich bulk endosomes from primary cultures of cerebellar granule neurons (CGNs). We first enriched bulk endosomes from CGNs using a classical subcellular fractionation approach (14, 15). Bulk endosomes were generated in CGNs via stimulation with 50 mM KCl in the presence of the fluorescent dye FM1-43 to label invaginating membrane. This stimulation protocol triggers both ADBE and CME to a similar extent as a train of high-frequency action potentials (16). After washing off FM1-43 and perfusion of ice-cold buffer (to arrest any trafficking processes), CGNs were mechanically lysed using a ball-bearing cell cracker. A postnuclear supernatant (PNS) containing intracellular

Significance

The maintenance of neurotransmission by synaptic vesicle (SV) recycling is critical to brain function. The dominant SV recycling mode during intense activity is activity-dependent bulk endocytosis (ADBE), suggesting it will perform a pivotal role in neurotransmission. However, the role of ADBE is still undetermined, due to the absence of identified molecules specific for this process. The determination of the bulk endosome proteome (a key ADBE organelle) revealed that it has a unique molecular signature and identified a role for Rab11 in presynaptic function. This work provides the molecular inventory of ADBE, a resource that will be of significant value to researchers wishing to modulate neurotransmission during intense neuronal activity in both health and disease.

Author contributions: A.C.K., M.T., and M.A.C. designed research; A.C.K., J.P., and E.C.D. performed research; A.C.K., J.P., and M.T. analyzed data; and A.C.K., M.T., and M.A.C. wrote the paper.

The authors declare no conflict of interest.

This article is a PNAS Direct Submission.

[1]To whom correspondence should be addressed. Email: m.cousin@ed.ac.uk.

This article contains supporting information online at www.pnas.org/lookup/suppl/doi:10.1073/pnas.1809189115/-/DCSupplemental.

Published online October 9, 2018.

organelles was prepared from this CGN lysate and then subjected to discontinuous subcellular fractionation using Nycodenz gradients (Fig. 1*A*). The Nycodenz fractionation protocol efficiently separates endosomes from SVs, with endosomes enriched between the 12 and 20% interface and SVs between the 20 and 25% interface (14, 15). In agreement, an increase in FM1-43 signal was visualized in the 12 and 20% interface fraction, suggesting that bulk endosomes were enriched via this approach (Fig. 1*B*). Increased FM1-43 fluorescence was also observed at the 20 and 25% Nycodenz interface, suggesting this fraction contained SVs (15). The presence of bulk endosomes and SVs in their respective Nycodenz fractions was confirmed by performing an identical protocol, but this time using the fluid-phase marker horseradish peroxidase (HRP) instead of FM1-43. HRP was converted to an electron-dense reaction product to visualize endocytic structures with bulk endosomes located in the 12 and 20% interface, whereas SVs were in the 20 and 25% interface (Fig. 1 *C–F*). Previous quantification of the number of HRP-labeled bulk endosomes and SVs confirmed that these structures were enriched in their respective subcellular fractions (15) and were absent from other fractions (*SI Appendix*, Fig. S1). Therefore, we confirmed the biochemical enrichment of bulk endosomes by two independent methods.

After confirming the enrichment of bulk endosomes at the 12 and 20% Nycodenz interface, three independent preparations of this subcellular fraction were subjected to liquid chromatography-tandem mass spectrometry (LC-MS/MS) analysis. A total of 1,026 proteins were identified from these samples in at least two out of the three replicates (a full list is presented in Dataset S1). To determine whether identified proteins shared either specific cell functions or localizations, these hits were subjected to cluster analysis using the Database for Annotation, Visualization and Integrated Discovery (DAVID) (17, 18) (Fig. 1*G*). DAVID functional annotation clustering analysis creates clusters and subclusters for proteins that have similarity in a biological function by extracting information from a variety of databases, including the gene ontology (GO) database. Each cluster, given a descriptive name, can have various subclusters, which are displayed as different-colored boxes in the histogram in Fig. 1*G*. Importantly, the same protein can be present in multiple clusters. For example, a Rab GTPase would be present in a GTP-binding cluster and in subsequent nucleotide-binding, GTPase activity, and small GTPase subclusters. The most important element of the analysis is the DAVID enrichment score (Fig. 1*G*), which is based on the individual subclusters' score and directly correlates with the enrichment of the subclusters.

DAVID analysis revealed that the two top enriched clusters were cell adhesion and synapse, confirming enrichment of synaptic proteins (Dataset S5). A GO enrichment analysis (19, 20) was also applied to the same dataset (*SI Appendix*, Fig. S2). Cellular compartment analysis revealed a strong annotation for myelin sheath and focal adhesion compartments, with cadherin binding and actin filament binding top groupings within the molecular function category (*SI Appendix*, Fig. S2). Thus, via two independent bioinformatic analyses, bulk endosomes purified via biochemical fractionation have a strong link to cell-adhesion molecules and synaptic function.

The Molecular Inventory of Bulk Endosomes Enriched via Magnetic Purification. Both optical and morphological assays confirmed that bulk endosomes were enriched in the Nycodenz fraction submitted for MS analysis; however, this fraction may also contain other endosomal subtypes such as early, recycling, or late endosomes (14). Therefore, to determine which molecules detected via Nycodenz fractionation were derived specifically from bulk endosomes, we enriched these structures via an additional independent approach. In this protocol, bulk endosomes were purified using magnetic columns after their fluid-phase labeling with 10-nm-diameter iron nanoparticles. The stochastic uptake of these particles into SVs is very inefficient, due to the small internal diameter of an SV (25 nm), meaning the great majority of particles will be accumulated via ADBE. The protocol for bulk endosome generation was identical to that described for the FM1-43 fractionation studies, with the exception that the iron nanoparticles were present during the stimulation period (Fig. 2*A*). After mechanical cell lysis, the PNS containing iron particle-labeled bulk endosomes was passed through magnetic columns. Retained bulk endosomes were then eluted from these columns by removal from the magnetic source and subsequently processed for electron microscopy to confirm the presence of bulk endosomes. When these samples were visualized, iron nanoparticles were observed inside membrane structures that were larger than 100 nm, confirming bulk endosome enrichment (Fig. 2 *B–D* and *SI Appendix*, Fig. S3). Furthermore, an enrichment of known ADBE molecules was observed in samples extracted from stimulated neuronal cultures (*SI Appendix*, Fig. S4).

The proteome of bulk endosomes purified via magnetic nanoparticles was then analyzed using an identical LC-MS/MS approach. A total of 1,284 molecules were identified from three independent preparations (Dataset S2). Cluster analysis using DAVID annotations revealed the top two clusters enriched were identical to those identified with the Nycodenz fractionation protocol, synapse and cell adhesion. In addition, other enriched clusters were cytoskeleton and GTP binding (Fig. 2*E* and Dataset S6). When GO enrichment analysis was performed, a very similar annotation for functions and compartments was found compared with endosomes enriched via subcellular fractionation, including myelin sheath as the top compartment and GDP binding as the top molecular function (*SI Appendix*, Fig. S5).

Parallel Enrichment Protocols Reveal the ADBE Proteome. We next compared the molecules identified via these two independent enrichment protocols. There was a high degree of convergence between these two datasets. A total of 894 proteins were quantified in at least two out of three replicates in both samples (Dataset S4), indicating that more than 77% of the proteins identified were found in both samples (Fig. 3*A*; excluded proteins from both enrichment protocols are displayed in *SI Appendix*, Fig. S6). Unsurprisingly, DAVID analysis revealed the top two enriched clusters were synapse and cell adhesion, with cytoskeleton and GTP binding the next most enriched (Fig. 3*B* and Dataset S7). The common proteins identified via these two independent enrichment protocols therefore form the molecular inventory of the bulk endosome, which we have termed the ADBE proteome.

To determine what the key functional networks may be within the ADBE proteome, the interactions of these core proteins were extracted from the STRING database (21). Proteins strongly interacting in this network were retained and arranged according to their function and localization. This analysis revealed a series of network hubs, with Rab proteins at their core (Fig. 4). This is not surprising, since Rab proteins perform a series of essential roles to ensure the specificity and directionality of intracellular vesicle trafficking between multiple compartments (12, 22). Vesicle trafficking formed one of the largest hubs, which contained a series of SV cargo proteins. This was expected, since SVs are generated from bulk endosomes, meaning they should contain molecules required to generate a functional SV (2). The V-ATPase hub contained the majority of the V-ATPase subunits required for both SV and endosome acidification (23). This was again expected, since V-type ATPase-mediated acidification is essential for SV generation from bulk endosomes (24). Another large hub is the actin cytoskeleton, which has been intimately linked to ADBE by a series of studies (6, 25–28). Therefore, these network hubs indicate the enrichment of the key presynaptic recycling organelle, bulk endosomes.

Other network hubs were the signaling, chaperone, endoplasmic reticulum (ER), and catenin hubs. The chaperone hub contained both Hsp70 and Hsp90 family members. Hspa4/5/8/12 are members of the Hsp70 family that participate in clathrin-coated vesicle (CCV) uncoating (29, 30), whereas Stip1 mediates the association of Hsc70 and Hsp90 and acts as a scaffold for the essential ADBE

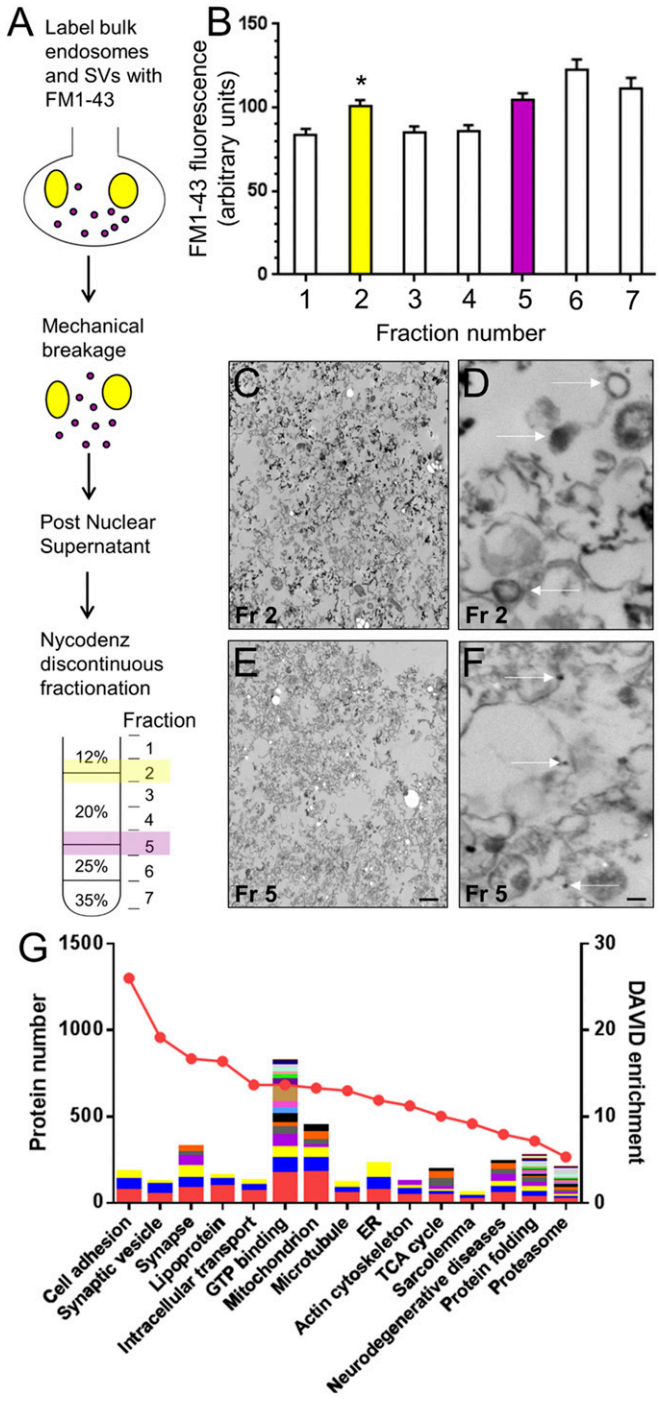

Fig. 1. Bulk endosome proteome generated via Nycodenz fractionation. (*A*) Protocol for enrichment of bulk endosomes. Primary cultures of cerebellar granule neurons were stimulated using 50 mM KCl for 2 min in the presence of 10 μM FM1-43. Cells were washed thoroughly, harvested, and lysed mechanically using a ball-bearing cell cracker. The postnuclear supernatant was generated and submitted to subcellular fractionation using discontinuous Nycodenz gradients (12, 20, 25, and 35%). (*B*) Seven fractions were obtained (1 to 7) and their fluorescence was quantified after normalization to the PNS fraction (normalized to 900 arbitrary units). Fraction 2 (yellow) and fraction 5 (purple) are highlighted since they contain bulk endosomes and SVs, respectively (all $n = 6 \pm$ SEM, $^*P < 0.05$, one-way ANOVA fractions 1 to 4). (*C*–*F*) An identical protocol was performed to load 10 mg/mL HRP into bulk endosomes and SVs. After conversion of HRP to an electron-dense product, fractions 2 (Fr 2) and 5 (Fr 5) were visualized by transmission electron microscopy. Low- (*C* and *E*) and high- (*D* and *F*) magnification images are displayed. [Scale bars, 2 μm (*C* and *E*) and 200 nm (*D* and *F*).] Arrows indicate HRP-labeled structures in *D* and *F*. (*G*) Fraction 2 was subjected to LC-MS/MS analysis and the results were processed using DAVID functional annotation clustering analysis. The top 15 enriched clusters are displayed in descending order of their DAVID enrichment score on the right *y* axis. The number of proteins in each DAVID cluster is presented on the left *y* axis. Subclusters are represented as different colors. It should be noted that proteins can be represented multiple times both within and between DAVID clusters and subclusters, meaning the protein number is not a representation of the independent number of proteins per cluster.

kinase GSK3β (31, 32). Hsp90 members regulate vesicle trafficking via regulating Rab GTPases (33, 34). The T-complex protein (TCP) complex is part of the chaperonin complex, which is linked to protein clearance in concert with the actin cytoskeleton (35). The ER and catenin hubs are also of interest, since catenins participate in both synapse formation and SV localization (36–38). Furthermore, the ER forms contacts with both the plasma membrane and endosomes within nerve terminals (39) and controls presynaptic function (40).

Other network hubs included metabolism, G-protein signaling, and mitochondria. The presence of a high proportion of metabolic enzymes is not unexpected, since the SV proteome contains a similar enrichment in these enzymes (41). Furthermore, a series of glycolytic enzymes are found on vesicles during their trafficking (42, 43) and are recruited to the presynapse during neuronal activity (44). This supports recent studies demonstrating that SV endocytosis has the highest energy demand within the presynapse (45). The large, central G protein-signaling hub is intriguing, suggesting specific presynaptic G protein-coupled receptors perform a regulatory role in ADBE (46, 47). In support, ADBE is negatively regulated by the extracellular signaling molecule BDNF (11), indicating the potential for plasma membrane receptors to modulate this endocytosis mode. The mitochondrial hub suggested potential contamination from this organelle; however, a potential link to ADBE cannot be eliminated at this stage.

The remaining hubs reveal potentially intriguing processes and molecules for future study. For example, peroxiredoxins impact on ER–endosome signaling (48) and interact with endosomal molecules such as phosphatidylinositol 4-kinase IIα, BLOC-1, and AP-3 (49). Similarly, the proteasome has been implicated in presynaptic function and SV recycling (50, 51), whereas both mono- and polyubiquitination have been linked to SV protein degradation and trafficking (52). Some 14-3-3 protein isoforms within the 14-3-3 hub have an SV localization, and are molecules that act in a series of presynaptic signaling cascades (53), including the ADBE kinases phosphatidylinositol 3-kinase and GSK3β (9, 54). The presence of the plasma membrane ATPase hub is intriguing, suggesting that cargo retrieval via ADBE may not be as accurate or precise as that during CME. In support, a $GABA_A$ receptor hub was also identified, which may either be a contaminant or alternatively indicate the presence of presynaptic $GABA_A$ receptors (55). However, the majority of $GABA_A$ receptors on CGNs appear to be extrasynaptic and located at somato–dendritic contacts (56). Finally, a flotillin hub was identified. Flotillins copurify with SVs (41) and promote glutamatergic synapse development (57). They are also required for clathrin-independent endocytosis in nonneuronal cells (58) and participate in cytoskeleton function and cell adhesion (59). These network hubs may therefore reveal information about processes and molecules essential for ADBE.

Rab11 Increases the Number of Nerve Terminals Performing ADBE. GTP-binding proteins were one of the largest clusters within the ADBE proteome, with a Rab small GTPase cluster also enriched (Fig. 3*B*). Furthermore, 15 discrete Rab GTPases were identified as a key interaction hub within the ADBE proteome (Fig. 4 and Table 1). This enrichment of Rab proteins, in addition to the fact that ADBE appears to have multiple uncharacterized endosome trafficking stages (60), prompted us to determine whether they performed specific roles in ADBE. To address this, we selected a

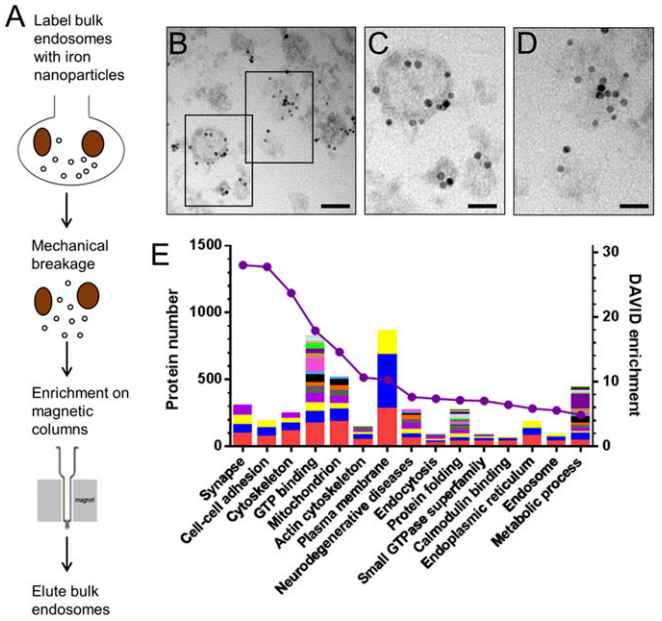

Fig. 2. Bulk endosome proteome generated via iron nanoparticle isolation. (*A*) Protocol for enrichment of bulk endosomes. Primary cultures of CGNs were stimulated using 50 mM KCl for 2 min in the presence of 1 mg/mL 10-nm iron nanoparticles. Cells were washed thoroughly, harvested, and lysed mechanically using a ball-bearing cell cracker. The postnuclear supernatant was generated and applied to magnetic columns. Retained bulk endosomes were eluted by removal from the magnet and processed for either electron microscopy or mass spectrometry analysis. (*B–D*) Representative images of the eluted bulk endosome fraction at either low- (*B*) or high- (*C* and *D*) magnification are displayed. [Scale bars, 250 nm (*B*) and 100 nm (*C* and *D*).] (*E*) Eluted bulk endosomes were subjected to LC-MS/MS analysis and the results were processed using DAVID functional annotation clustering analysis. The top 15 enriched clusters are displayed in descending order of their DAVID enrichment score on the right *y* axis. The number of proteins in each DAVID cluster is presented on the left *y* axis.

subset for further study. These were the early endosomal marker Rab5, the late endosomal protein Rab7, the ER-Golgi protein Rab10, and finally a key effector of tubular recycling endosomes, Rab11. We investigated both wild-type and constitutively active forms of these Rabs, since their GTP binding state are key to their biological function (13).

We first determined the distribution of wild-type Rabs in CGNs using coefficient of variation (CV) analysis. CV analysis reports the variability of the fluorescent signal along the axon (61, 62), thus inferring whether these Rabs are localized in clusters or are diffusely distributed. All Rabs were fused to the fluorescent protein mCerulean (mCer) to allow visualization of their distribution. The majority of Rabs had a diffuse cytosolic localization pattern, as evidenced by a low CV score equivalent to the empty mCer vector (Fig. 5 *A* and *B*). The exception to this was mCer-Rab7$_{WT}$, which displayed a significant enrichment in axonal puncta (Fig. 5 *A* and *B*) comparable to that of the SV protein synaptophysin (*SI Appendix*, Fig. S7). This enrichment was not increased when the constitutively active mutant (Q67L) was expressed, suggesting the permanent presence of Rab7 compartments along the axon. Interestingly, constitutively active Rab5 (Q79L) and Rab11 (Q70L) mutants displayed a significant enrichment in axonal puncta compared with their wild-type equivalents (Fig. 5 *A* and *B*). The number of Rab clusters is invariant along the axon (*SI Appendix*, Fig. S8), suggesting that activation of both Rab5 and Rab11 triggers their recruitment to axonal clusters, potentially corresponding to nerve terminals.

To confirm that the observed increase in CV was due to a recruitment of activated Rabs to nerve terminals along axons, we performed colocalization analysis using the presynaptic active zone and SV markers bassoon and SV2A, respectively. All wild-type Rabs demonstrated good colocalization with nerve terminals (Fig. 5 *D* and *E*), in agreement with previous studies (63). When constitutively active versions were analyzed, ~75% of mCer-Rab5$_{Q79L}$, mCer-Rab7$_{Q67L}$, and mCer-Rab11$_{Q70L}$ colocalized with these presynaptic markers, with Rab5 and Rab11 demonstrating a small enrichment compared with wild type (Fig. 5 *C–E*). In contrast, mCer-Rab10$_{Q68L}$ colocalization with either bassoon or SV2A was reduced (Fig. 5 *C–E*). Therefore, a high percentage of active Rab5, Rab7, and Rab11 are present in nerve terminals (63), suggesting they may perform a role in presynaptic function.

To determine whether these specific Rabs controlled ADBE, we first assessed the effect of overexpression of wild-type proteins on bulk endosome formation during intense neuronal activity. Bulk endosome formation was monitored via the uptake of a fluorescent 40-kDa dextran [tetramethylrhodamine (TMR)-dextran] that selectively reports ADBE due to size exclusion from SVs (16) (Fig. 6*A* and *SI Appendix*, Fig. S9). TMR-dextran was coapplied during a train of 400 action potentials delivered at 40-Hz stimulation, a stimulus that maximally triggers ADBE (7). There was no significant change in the number of nerve terminals performing activity-dependent TMR-dextran uptake for any

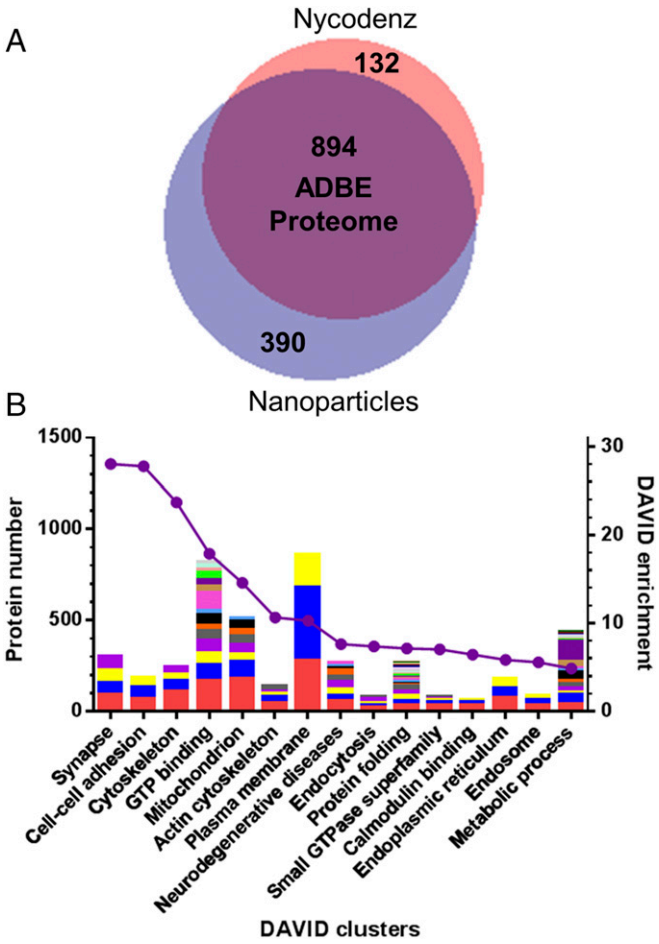

Fig. 3. ADBE proteome. (*A*) Venn diagram illustrating the degree of similarity between the two proteomes derived from independent bulk endosome enrichment protocols. (*B*) The consolidated ADBE proteome was processed using DAVID functional annotation clustering analysis. The top 15 enriched clusters are displayed in descending order of their DAVID enrichment score on the right *y* axis. The number of proteins in each DAVID cluster is presented on the left *y* axis.

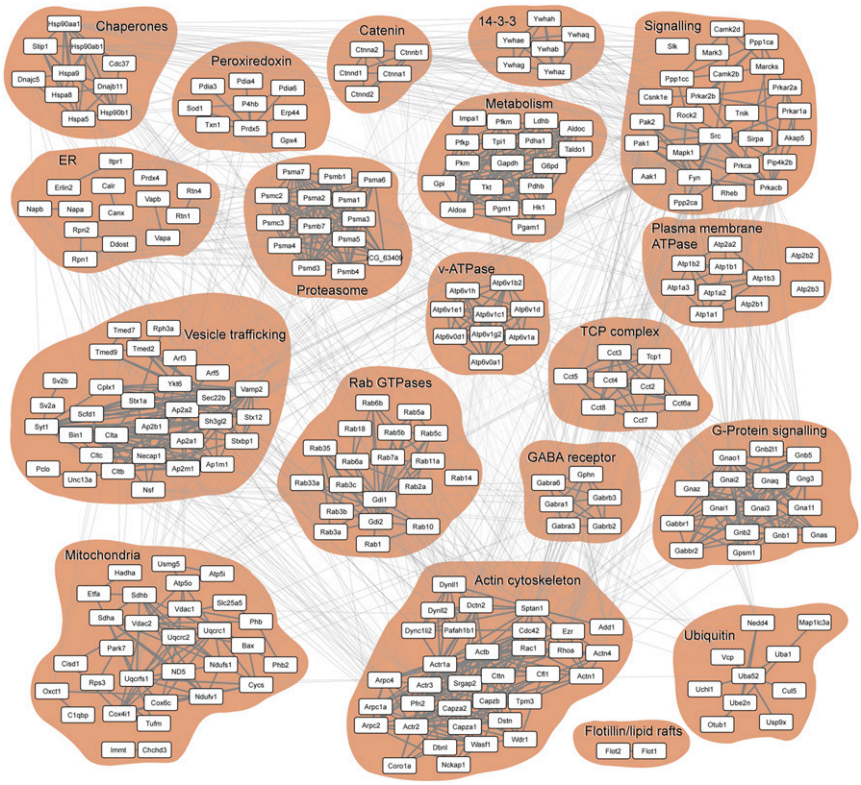

Fig. 4. Core ADBE proteome network. Protein–protein interactions of the consolidated ADBE proteome were extracted from the STRING database. A network was arranged according to selected functions and localization, presenting the most enriched hubs and strongest interactions.

wild-type Rab protein, suggesting that increased dosage of these GTPases has no effect on ADBE (Fig. 6*B*).

We next determined whether the constitutively active form of these Rabs influenced ADBE, since we observed enhanced localization to nerve terminals when they were in their GTP-bound state. When activity-dependent TMR-dextran uptake was assessed in these neurons, mCer-Rab11$_{Q70L}$ significantly increased the number of nerve terminals performing ADBE (Fig. 6*C*). In contrast, all of the other Rab mutants had no effect (Fig. 6*C*). The dominant-negative form of Rab11 (S25N) robustly inhibited the uptake of TMR-dextran (*SI Appendix*, Fig. S10), in agreement with a key role for Rab11 in the triggering of ADBE in central nerve terminals.

To confirm that Rab11$_{Q70L}$ increased the number of nerve terminals performing ADBE, we corroborated this finding via a complementary approach, using the fluorescent genetically encoded reporter VAMP4-pHluorin (VAMP4-pH) (64). VAMP4-pH tracks the occurrence of ADBE at individual nerve terminals, since it is selectively trafficked via this endocytosis mode during elevated neuronal activity (15). It reports the pH of its immediate environment by virtue of a pH-sensitive GFP moiety (pHluorin) fused to its C-terminal luminal domain. VAMP4-pH that is localized at the plasma membrane is therefore fluorescent, due to the neutral pH of the extracellular medium; however, its fluorescence is quenched within an acidic environment, such as an SV or bulk endosome. Triggering of ADBE therefore results in plasma membrane VAMP4-pH being captured into newly formed and slowly acidifying bulk endosomes. This process is reported as a prolonged decrease in fluorescence that occurs over the time course of minutes (Fig. 6*D*) (15). However, in nerve terminals where ADBE is not recruited, the fluorescence of VAMP4-pH slowly increases after stimulation. This slow fluorescence increase reflects asynchronous release—for which VAMP4 is also essential (65). Therefore, by classifying VAMP4-pH responses from individual nerve terminals as those that display asynchronous release (i.e., traces with an upward trajectory) and those that undergo ADBE (traces with a downward trajectory), the number of nerve terminals performing ADBE can be monitored (Fig. 6*D*).

When CGNs expressing the empty mCer vector and VAMP4-pH were challenged with a train of high-frequency action potentials (40 Hz, 10 s), ~25% of nerve terminals displayed a slow VAMP4-pH downstroke (Fig. 6*E*). When this experiment was repeated in neurons expressing mCer-Rab11$_{Q70L}$, there was a significant increase in the number of nerve terminals displaying a slow VAMP4-pHluorin

Table 1. Identified Rab proteins within the core ADBE proteome

Rab protein	UniProt identifier
Rab1a	Q6NYB7
Rab2a	F1LP82
Rab3a	P63012
Rab3b	Q63941
Rab3c	P62824
Rab45	D4ADS8
Rab5a	M0RC99
Rab5b	A1L1J8
Rab5c	B0BNK1
Rab6a	A0A0H2UHP9
Rab6b	A0A0G2JT78
Rab7a	P09527
Rab10	P35281
Rab11a	P62494
Rab14	B0BMW0
Rab18	Q5EB77
Rab21	Q6AXT5
Rab23	D3ZRM5
Rab33a	D3ZCU8
Rab35	Q5U316

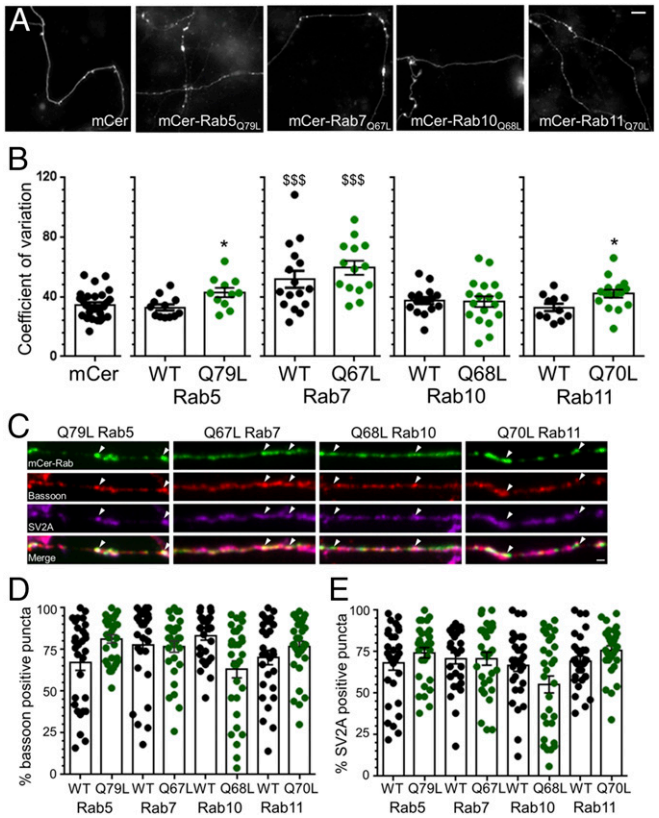

Fig. 5. Constitutively active Rab11 is recruited to nerve terminals. Primary cultures of CGNs were transfected with either mCerulean empty vector (mCer), wild-type (WT), or constitutively active (CA) versions of mCer-tagged Rab GTPases (Q79L Rab5, Q67L Rab7, Q68L Rab10, and Q70L Rab11). (*A*) Representative images of neurons transfected with either mCer or CA mCer-tagged Rabs. (Scale bar, 1 μm.) (*B*) Coefficient of variation analysis of transfected neurons. $^{\$\$\$}P < 0.001$, one-way ANOVA across all WT or CA Rab neurons. $^{*}P < 0.05$, Student's *t* test WT vs. CA Rabs (mCer, $n = 29$; WT Rab5, $n = 12$; Q79L Rab5, $n = 11$; WT Rab7, $n = 16$; Q67L Rab7, $n = 14$; WT Rab10, $n = 16$; Q68L Rab10, $n = 18$; WT Rab11, $n = 11$; Q70L Rab11, $n = 16$ neurons). (*C–E*) CGNs were transfected with either wild-type or CA versions of mCer-tagged Rab5, Rab7, Rab10, or Rab11 and costained for bassoon and SV2A. (*C*) Representative images illustrate the location of CA Rabs with respect to nerve terminals (mCer-Rab, green; bassoon, red; SV2A, purple). Arrowheads indicate Rab puncta. (Scale bar, 1 μm.) (*D* and *E*) Quantification of the percentage of Rab puncta (±SEM) that colocalize with either bassoon (*D*) or SV2A (*E*); $n = 30$ neurons in all cases.

downstroke (Fig. 6*E*). Therefore, we have shown via two independent approaches that $Rab11_{Q70L}$ increases the number of nerve terminals performing ADBE, and therefore may be a key molecule in determining when and where this endocytosis mode is triggered.

Rab11 Accelerates CME During Intense Neuronal Activity. One potential mechanism for the increased prevalence of ADBE is an increase in the number of SVs fusing, providing an increased endocytic load (66). To determine this, we monitored SV exocytosis using synaptophysin-pHluorin (syp-pH) (3). Syp-pH has a pHluorin moiety fused to an intraluminal loop of the SV protein synaptophysin. Similar to VAMP4-pH, its fluorescence is quenched by acidic environments such as the interior of an SV. However, since the great majority of syp-pH is expressed on SVs, it displays a completely different fluorescence profile from VAMP4-pH during action potential stimulation. Neuronal activity results in syp-pH dequenching due to SV fusion (exocytosis), resulting in an increase in fluorescence, therefore reporting the extent of SV fusion during an action potential train (Fig. 7*A*). To estimate the number of SVs fusing as a proportion of the total SV pool, cultures were challenged with an ammonium chloride solution, which unquenches all SVs inside the nerve terminal. When this protocol was performed, no significant change in the extent of the evoked syp-pH peak response was observed when neurons expressing mCer empty vector and mCer-$Rab11_{Q70L}$ were compared (Fig. 7*B*). This suggested that there was no effect of $Rab11_{Q70L}$ on SV exocytosis. To confirm this, experiments were performed in the presence of the V-type ATPase inhibitor bafilomycin A1, which allows SV fusion events to be visualized independent from SV endocytosis. These experiments confirmed that expression of $Rab11_{Q70L}$ had no effect on SV exocytosis during intense neuronal activity (Fig. 7*C* and *SI Appendix*, Fig. S11*A*), eliminating an increase in the number of SVs fusing as an explanation for the increased number of nerve terminals performing ADBE.

After neuronal activity terminates, syp-pH fluorescence is requenched by SV acidification after its retrieval by CME. CME kinetics can be estimated by monitoring the rate of fluorescence decrease poststimulation (67), since SV acidification is not rate-limiting in this process (68) (but see ref. 69). Importantly, the amount of syp-pH retrieved by ADBE is minimal, even during intense stimulation (15), ensuring that it is an accurate reporter of CME. The syp-pH response can therefore also be interrogated for potential effects of $Rab11_{Q70L}$ on CME, by normalizing to the peak fluorescence response and monitoring the rate of fluorescence recovery poststimulation. When this analysis was performed there was an acceleration of syp-pH recovery in mCer-$Rab11_{Q70L}$–expressing cells compared with mCer alone (Fig. 7*D*), suggesting an increase in the speed of CME. This was confirmed using two independent parameters. First, in mCer-$Rab11_{Q70L}$–expressing neurons, the time constant of syp-pH retrieval was significantly lowered (Fig. 7*E*), and second, the extent of syp-pH retrieval was reduced 1 min after stimulation (*SI Appendix*, Fig. S11*E*). This acceleration of CME was only observed during intense neuronal activity, since there was no effect of mCer-$Rab11_{Q70L}$ expression on either the evoked syp-pH peak height (*SI Appendix*, Fig. S11 *B–D*) or syp-pH retrieval during mild activity. Therefore, $Rab11_{Q70L}$ has two activity-dependent effects on the SV life cycle: an increase in the number of nerve terminals performing ADBE and an acceleration of an ADBE-independent form of endocytosis, most likely CME.

Discussion

The ADBE Proteome. We have cataloged the molecular inventory of the bulk endosome using two independent methods to enrich these key organelles, and in doing so have revealed the ADBE proteome. Bioinformatic analysis revealed that in addition to the expected complement of SV and endosomal proteins, there was a high prevalence of cytoskeletal, metabolic, and signaling molecules. One of the most abundant classes of molecules were GTP-binding proteins, with Rab GTPases specifically enriched. STRING network analysis revealed that the ADBE proteome had a Rab network hub at its center, suggesting that these GTPases may perform a role in this process. Using this information, we uncovered a specific role for Rab11 in the triggering of ADBE.

An essential aspect of both bulk endosome enrichment protocols was the use of a near-homogeneous source of neuronal material. We selected primary cultures of CGNs for this purpose, since they can be cultured to high homogeneity (70). This minimizes the variability often associated with other primary neuronal culture systems or from biochemical preparations such as isolated nerve terminals from whole brains (synaptosomes). Substantial amounts of tissue can be obtained from this preparation (~10 million CGNs can be obtained from one postnatal day 7 rat pup). This makes endosome isolation feasible from a primary neuronal culture system in a manner that would not be possible for another preparation such as hippocampal neurons. Finally and importantly, ADBE has also been extensively characterized in this culture system (7–9, 11, 15, 71).

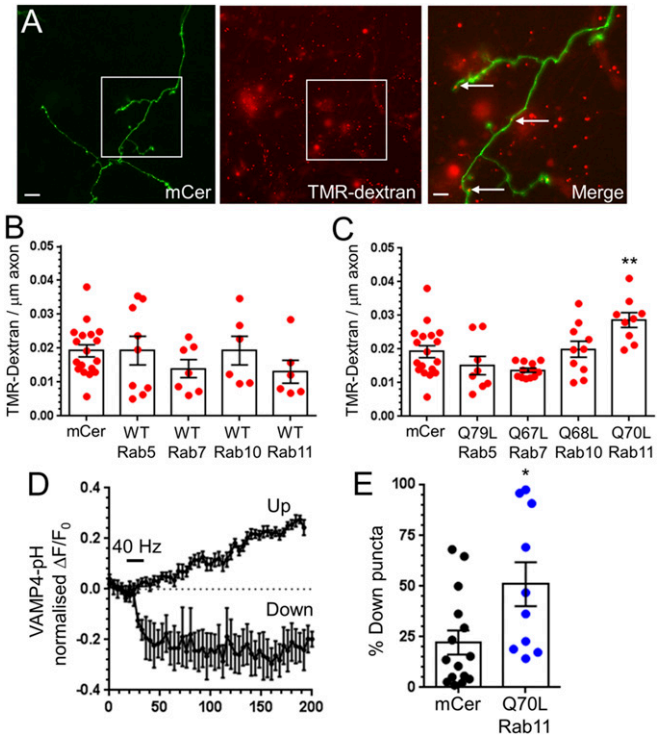

Fig. 6. Constitutively active Rab11 facilitates ADBE. Primary cultures of CGNs were transfected with either mCerulean empty vector (mCer), WT, or constitutively active versions of mCer-tagged Rab GTPases (Q79L Rab5, Q67L Rab7, Q68L Rab10, and Q70L Rab11). After 3 d, transfected neurons were stimulated with a train of 400 action potentials (40 Hz) in the presence of 50 µM TMR-dextran. TMR-dextran was immediately washed away and images were acquired. (*A*) Representative images of neurons transfected with mCer (green), loaded with TMR-dextran (red), and overlaid (Merge). [Scale bars, 2 µm (mCer and TMR-dextran) and 0.5 µm (Merge).] Arrows indicate TMR-dextran uptake in transfected neurons. (*B* and *C*) TMR-dextran uptake per 1 µm of axon is displayed for mCer-tagged WT (*B*) or mutant (*C*) Rab-expressing neurons ± SEM (**$P < 0.01$, one-way ANOVA; mCer, $n = 18$; WT Rab5, $n = 9$; Q79L Rab5, $n = 8$; WT Rab7, $n = 7$; Q67L Rab7, $n = 12$; WT Rab10, $n = 6$; Q68L Rab10, $n = 10$; WT Rab11, $n = 6$; Q70L Rab11, $n = 9$ coverslips). (*D* and *E*) CGNs were transfected with VAMP4-pHluorin and either mCer or mCer-Rab11$_{Q70L}$. After 3 d, cultures were stimulated with a single train of 400 action potentials delivered at 40 Hz followed by a pulse of ammonium chloride buffer (NH_4Cl). (*D*) The VAMP4-pH response is displayed for mCer-transfected neurons, grouped into nerve terminals that displayed either "Up" or "Down" fluorescence profiles ($\Delta F/F_0$ ± SEM). Stimulation is indicated by the bar. Down represents the occurrence (but not amount) of ADBE. (*E*) Quantification of the number of down responses in either mCer or mCer-Rab11$_{Q70L}$ neurons ± SEM (mCer, $n = 15$; mCer-Rab11$_{Q70L}$, $n = 10$ coverslips; *$P < 0.05$, Student's t test).

One other group has attempted to purify endosomes from whole mouse cortex using fractionation on a continuous density gradient (72). However, this study separated endosomes into "early" and "late" by blotting for classical marker proteins. It also compared the protein complement of endosomes derived from either wild type or an AP-1/σ1-B knockout mouse model [which accumulates synaptic endosomal structures (73)]. It is difficult to correlate these results with ours, since the experimental n was limited to one for each condition and there was no activity-dependent formation of bulk endosomes.

A number of molecules are essential for ADBE function, such as syndapin, dynamin, calcineurin, GSK3, synaptotagmin-7, VAMP4, AP-1, AP-2, and AP-3 (9, 15, 60, 71, 74, 75). Importantly, all were identified within the ADBE core proteome, with the exception of VAMP4. The absence of VAMP4 was not surprising, since previous proteomic studies examining SVs identified difficulties in detection via mass spectrometry (41, 76, 77). We confirmed the strong presence of VAMP4 within the ADBE proteome by Western blotting (*SI Appendix*, Fig. S12). A specific aim of this study was to identify molecules that were unique to ADBE, since their identification should allow a more selective intervention to determine the physiological role of this endocytosis mode. Within the ADBE proteome, three proteins were found that have no currently identified function. Minimal information is present for these proteins: One is predicted to be a cytoplasmic protein, one has a putative transmembrane domain, and the final protein is a catenin-like protein. An urgent priority is now to determine whether these molecules are required for ADBE and, critically, whether they are unique to this process.

Rab11 Has Activity-Dependent Roles in ADBE and CME. One of the central hubs within the ADBE proteome was Rab GTPase. The large number of Rab proteins detected within the ADBE proteome (total of 15) was initially surprising; however, compared with the proteome of purified SVs, it is actually less than that found on SVs [a total of 25 (41)]. These two subsets of molecules are highly similar, with 70% of Rabs detected in both. A previous study has investigated the function of Rabs identified on purified SVs—the SV "Rabome" (63). This study identified 21 different SV Rabs by MS, again resulting in 70% coverage of the ADBE proteome. A third study that investigated the proteome of either glutamatergic or GABAergic SVs identified 17 different Rabs in total, with 75% similarity to the ADBE Rabome (77). Therefore, bulk endosomes contain a specific subset of Rab molecules that are also located on SVs.

We found that Rab11$_{Q70L}$ increased the number of nerve terminals performing ADBE. This effect was not due to increased SV exocytosis, since Rab11$_{Q70L}$ did not impact on this parameter. Rab11$_{Q70L}$ preferentially localizes to nerve terminals, as does

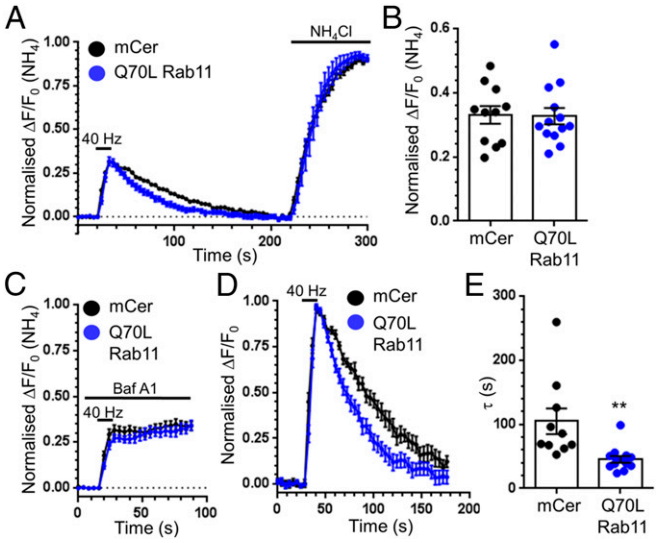

Fig. 7. Constitutively active Rab11 accelerates CME. (*A*, *B*, *D*, and *E*) Primary cultures of CGNs were transfected with synaptophysin-pHluorin and either mCerulean empty vector (mCer) or Q70L Rab11 (mCer-Rab11$_{Q70L}$). After 3 d, cultures were stimulated with a single train of 400 action potentials delivered at 40 Hz followed by a pulse of ammonium chloride buffer. Traces display the time course of the average fluorescent syp-pH response normalized to the total SV pool revealed by NH_4Cl (*A*; $\Delta F/F_0$ ± SEM) or normalized to stimulation (*D*; $\Delta F/F_0$ ± SEM). Black traces indicate mCer; blue traces indicate mCer-Rab11$_{Q70L}$. Bars indicate period of stimulation. Quantification of the evoked peak height (*B*) or the time constant (τ) of fluorescence decay poststimulation (*E*) are displayed ±SEM (mCer, $n = 11$; mCer-Rab11$_{Q70L}$, $n = 13$ coverslips). For both *B* and *E* a Student's t test was performed; **$P = 0.0042$. (*C*) An identical experiment was performed, though in this case neurons were incubated with bafilomycin A1 (1 µM) for 60 s before and also during and after stimulation (indicated by the bar). Traces display the time course of the average fluorescent syp-pH response normalized to the total SV pool revealed by NH_4Cl ($\Delta F/F_0$ ± SEM; mCer, $n = 18$; mCer-Rab11$_{Q70L}$, $n = 9$ coverslips).

endogenous Rab11 (*SI Appendix*, Fig. S13). Two independent protocols were used to monitor ADBE, TMR-dextran uptake and VAMP4-pH trafficking. All central nerve terminals have the ability to perform ADBE; however, only a fraction of these synapses undergo ADBE during a single action potential train (15, 16, 64, 78). TMR-dextran uptake identifies nerve terminals that perform ADBE, but not the amount of ADBE occurring per nerve terminal (16, 78), and therefore its output is binary. VAMP4-pH also reports the proportion of nerve terminals performing ADBE (64). This is because the fluorescence response from individual nerve terminals is a composite of ongoing bulk endosome acidification and asynchronous release. Since these opposing biological events contribute to the VAMP4-pH response, the magnitude of the fluorescent downstroke cannot be extrapolated to report the amount of ADBE occurring per nerve terminal. Both assays confirmed that expression of $Rab11_{Q70L}$ increased the number of nerve terminals performing ADBE.

An acceleration of a non-ADBE form of endocytosis was also observed in neurons expressing $Rab11_{Q70L}$. This mode is likely to be CME; however, a clathrin-independent, formin-dependent mode is also possible (6). The fact that this is only observed during intense neuronal activity suggests it is linked to the ADBE phenotype discussed above. However, it should be noted that inhibition of ADBE has little effect on the extent of CME (15). Therefore, it is premature to draw a causal relationship between these two Rab11-dependent effects. However, Rab11 activation does appear to facilitate both endocytosis modes.

Control of ADBE via Rab11. Rab11 classically facilitates the trafficking of cargo from the recycling endosome to the plasma membrane (12, 13). The requirement for Rab11 is both activity-dependent and acute, since SV turnover during low-frequency stimulation was unaffected and resting surface fraction of SV cargo was not altered (*SI Appendix*, Fig. S11*F*). Rab11 may act via tubular recycling endosomes in the presynapse, which have been identified in both mammalian (39) and invertebrate (79) nerve terminals. Therefore, one explanation for the increased occurrence of ADBE may be elevated flux through the endosomal trafficking system during intense neuronal activity.

Evidence of a potential role for Rab11 as a positive modulator of SV endocytosis comes mainly from model organisms (80, 81). How could Rab11 modulate SV recycling? One possibility is that the increased presynaptic localization of active Rab11 could recruit other factors to trigger ADBE. For example, the endosomal protein EHD-1 may be recruited by Rab11 via the intermediate Rab11FIP2 to provide a link between bulk endosomes and tubular recycling endosomes (82). In agreement, EHD-1 and its interaction partner, the essential ADBE protein syndapin (71, 83), are both present in the ADBE proteome and are located on tubular recycling endosomes (84). Alternatively, the apparent increase in ADBE could be due to increased mobility of bulk endosomes between nerve terminals. Movement of SV cargo and FM dyes between nerve terminals occurs immediately after SV recycling (85, 86), suggesting some of this traffic may be bulk endosomes. In agreement, the plus end-directed microtubule-based motor protein KIF13A [which interacts with GTP-Rab11 to promote formation and motility of recycling tubules (87)] is also found in the ADBE proteome, suggesting increased endosome mobility between nerve terminals may occur. These possibilities can only be directly addressed by a systematic interrogation of Rab11 regulators and targets, which will be the subject of ongoing research in our laboratory.

In summary, we have identified a subset of presynaptic molecules enriched on bulk endosomes and have termed this the ADBE proteome. This analysis has revealed potentially key roles for discrete neuronal processes and molecules for this endocytosis mode. Using this information, we revealed activity-dependent roles for Rab11 in both ADBE and CME. The determination of the ADBE proteome should provide a rich resource for future research into the cellular and physiological role of ADBE.

Materials and Methods

For information on materials, primary cell culture and transfections, TMR-dextran uptake, immunofluorescence labeling, electron microscopy, mass spectrometry, and protein interaction analysis, please refer to *SI Appendix*.

Imaging of pHluorin Responses. CGN cultures were removed from culture medium and left to repolarize for 10 min in incubation medium (170 mM NaCl, 3.5 mM KCl, 0.4 mM KH_2PO_4, 20 mM TES [*N*-Tris(hydroxymethyl)-methyl-2-aminoethane sulfonic acid], 5 mM $NaHCO_3$, 5 mM glucose, 1.2 mM Na_2SO_4, 1.2 mM $MgCl_2$, 1.3 mM $CaCl_2$, pH 7.4). Cultures were mounted in a Warner imaging chamber with embedded parallel platinum wires (RC-21BRFS) and placed on the stage of a Zeiss Axio Observer A1 epifluorescence microscope. Transfected neurons were visualized with a Zeiss Plan Apochromat 40× oil-immersion objective (N.A. 1.3) at 430-nm excitation (to visualize mCer), whereas pHluorin reporters were visualized at 500 nm (both using a dichroic >525-nm and long-pass emission filter, >535-nm). Cultures were subjected to continuous perfusion with incubation medium and stimulated with a train of either 400 action potentials delivered at 40 Hz (100 mA, 1-ms pulse width) or 300 action potentials delivered at 10 Hz where indicated. At the end of the experiment, cultures were challenged with alkaline imaging buffer (50 mM NH_4Cl substituted for 50 mM NaCl) to reveal total pHluorin fluorescence. Where indicated, cultures were also challenged with acidic imaging buffer (20 mM Mes substituted for 20 mM TES, pH 5.5). Fluorescent images were captured at 4-s intervals using a Zeiss AxioCam MRm Rev.3 digital camera and processed offline using ImageJ 1.43 software (NIH). Regions of interest of identical size were placed over nerve terminals and the total fluorescence intensity was monitored over time. Only regions that responded to action potential stimulation were selected for analysis. The pHluorin fluorescence change was calculated as $\Delta F/F_0$, and n refers to the number of individual coverslips examined. Statistical analyses were performed using Microsoft Excel and GraphPad Prism software.

Bulk Endosome Purification. For subcellular fractionation, CGN cultures were repolarized in incubation medium for 1 h to minimize existing bulk endosomes and were then stimulated for 2 min with 50 mM KCl in the presence of 10 μM FM1-43. Cells were washed once with incubation medium and then twice with incubation medium supplemented with 200 nM Advasep-7. CGNs were collected in an ice-cold buffer containing 250 mM sucrose, 3 mM imidazole (pH 7.4) and mechanically broken using a ball-bearing cell cracker (EMBL), with the lysate spun for 15 min at 1,200 × *g*. The postnuclear supernatant was deposited at the base of a discontinuous isosmotic Nycodenz gradient (12, 20, 25, and 35% in 3 mM imidazole, 0.5 mM EDTA, pH 7.4). The samples were centrifuged for 90 min at 170,000 × *g* in an Optima MAX-XP tabletop ultracentrifuge (Beckman Coulter). The different fractions were collected as indicated in Fig. 1*A*, with bulk endosomes located at the interface between 12 and 20% Nycodenz and SVs between 20 and 25% Nycodenz. The fluorescence of all fractions was monitored in a TD-700 fluorometer (Turner Designs) to reveal the presence of labeled compartments.

For magnetic isolation of bulk endosomes, CGNs were repolarized in incubation medium as above and stimulated with 50 mM KCl in the presence of 1 mg/mL 10-nm iron particles (Sigma-Aldrich; 725358). CGNs were lysed mechanically and PNS was acquired as outlined above. Magnetic columns (Miltenyi Biotec) were placed on a magnetic base (MiniMACS; Miltenyi Biotec) and primed with an ice-cold 250 mM sucrose, 3 mM imidazole (pH 7.4) solution. The PNS was then added to the column and the column was thoroughly washed using the previous solution including a protease inhibitor mixture and 1 mM PMSF. The column was then removed from the magnetic base and retained bulk endosomes were collected. This bulk endosome sample was concentrated in a chilled microfuge using a spin of 14,000 × *g* for 1 h.

Statistical Analysis. A Student's *t* test was performed for comparisons between two datasets. For comparisons between more than two datasets, a one-way ANOVA was employed. For comparisons between fluorescence responses over time, or where greater than one variable was being compared, a two-way ANOVA was performed.

ACKNOWLEDGMENTS. We thank Dr. Anetta Härtlova for supporting this work. This work was supported by a Wellcome Trust Investigator Award (to M.A.C.; 204954/Z/16/Z). A.C.K. was supported by a Marie Curie Initial Training Network Award (Project 289581–*NPlast*; to M.A.C.). M.T. was funded by Medical Research Council UK (Grant MC_UU_12016/5) and pharmaceutical companies supporting the Division of Signal Transduction Therapy (Boehringer-Ingelheim, GlaxoSmithKline, and Merck KGaA).

1. Kononenko NL, Haucke V (2015) Molecular mechanisms of presynaptic membrane retrieval and synaptic vesicle reformation. *Neuron* 85:484–496.
2. Kokotos AC, Cousin MA (2015) Synaptic vesicle generation from central nerve terminal endosomes. *Traffic* 16:229–240.
3. Granseth B, Odermatt B, Royle SJ, Lagnado L (2006) Clathrin-mediated endocytosis is the dominant mechanism of vesicle retrieval at hippocampal synapses. *Neuron* 51: 773–786.
4. Watanabe S, et al. (2013) Ultrafast endocytosis at mouse hippocampal synapses. *Nature* 504:242–247.
5. Watanabe S, et al. (2014) Clathrin regenerates synaptic vesicles from endosomes. *Nature* 515:228–233.
6. Soykan T, et al. (2017) Synaptic vesicle endocytosis occurs on multiple timescales and is mediated by formin-dependent actin assembly. *Neuron* 93:854–866.e4.
7. Clayton EL, Evans GJ, Cousin MA (2008) Bulk synaptic vesicle endocytosis is rapidly triggered during strong stimulation. *J Neurosci* 28:6627–6632.
8. Cheung G, Jupp OJ, Cousin MA (2010) Activity-dependent bulk endocytosis and clathrin-dependent endocytosis replenish specific synaptic vesicle pools in central nerve terminals. *J Neurosci* 30:8151–8161.
9. Clayton EL, et al. (2010) Dynamin I phosphorylation by GSK3 controls activity-dependent bulk endocytosis of synaptic vesicles. *Nat Neurosci* 13:845–851.
10. Koch D, et al. (2011) Proper synaptic vesicle formation and neuronal network activity critically rely on syndapin I. *EMBO J* 30:4955–4969.
11. Smillie KJ, Pawson J, Perkins EM, Jackson M, Cousin MA (2013) Control of synaptic vesicle endocytosis by an extracellular signalling molecule. *Nat Commun* 4:2394.
12. Wandinger-Ness A, Zerial M (2014) Rab proteins and the compartmentalization of the endosomal system. *Cold Spring Harb Perspect Biol* 6:a022616.
13. Hutagalung AH, Novick PJ (2011) Role of Rab GTPases in membrane traffic and cell physiology. *Physiol Rev* 91:119–149.
14. Barysch SV, Jahn R, Rizzoli SO (2010) A fluorescence-based in vitro assay for investigating early endosome dynamics. *Nat Protoc* 5:1127–1137.
15. Nicholson-Fish JC, Kokotos AC, Gillingwater TH, Smillie KJ, Cousin MA (2015) VAMP4 is an essential cargo molecule for activity-dependent bulk endocytosis. *Neuron* 88:973–984.
16. Clayton EL, Cousin MA (2009) Quantitative monitoring of activity-dependent bulk endocytosis of synaptic vesicle membrane by fluorescent dextran imaging. *J Neurosci Methods* 185:76–81.
17. Huang DW, et al. (2007) The DAVID Gene Functional Classification Tool: A novel biological module-centric algorithm to functionally analyze large gene lists. *Genome Biol* 8:R183.
18. Huang DW, Sherman BT, Lempicki RA (2009) Systematic and integrative analysis of large gene lists using DAVID bioinformatics resources. *Nat Protoc* 4:44–57.
19. Eden E, Lipson D, Yogev S, Yakhini Z (2007) Discovering motifs in ranked lists of DNA sequences. *PLoS Comput Biol* 3:e39.
20. Eden E, Navon R, Steinfeld I, Lipson D, Yakhini Z (2009) GOrilla: A tool for discovery and visualization of enriched GO terms in ranked gene lists. *BMC Bioinformatics* 10:48.
21. Szklarczyk D, et al. (2017) The STRING database in 2017: Quality-controlled protein-protein association networks, made broadly accessible. *Nucleic Acids Res* 45: D362–D368.
22. Grant BD, Donaldson JG (2009) Pathways and mechanisms of endocytic recycling. *Nat Rev Mol Cell Biol* 10:597–608.
23. Hnasko TS, Edwards RH (2012) Neurotransmitter corelease: Mechanism and physiological role. *Annu Rev Physiol* 74:225–243.
24. Cheung G, Cousin MA (2013) Synaptic vesicle generation from activity-dependent bulk endosomes requires calcium and calcineurin. *J Neurosci* 33:3370–3379.
25. Holt M, Cooke A, Wu MM, Lagnado L (2003) Bulk membrane retrieval in the synaptic terminal of retinal bipolar cells. *J Neurosci* 23:1329–1339.
26. Gormal RS, Nguyen TH, Martin S, Papadopulos A, Meunier FA (2015) An acto-myosin II constricting ring initiates the fission of activity-dependent bulk endosomes in neurosecretory cells. *J Neurosci* 35:1380–1389.
27. Richards DA, Rizzoli SO, Betz WJ (2004) Effects of wortmannin and latrunculin A on slow endocytosis at the frog neuromuscular junction. *J Physiol* 557:77–91.
28. Wu XS, et al. (2016) Actin is crucial for all kinetically distinguishable forms of endocytosis at synapses. *Neuron* 92:1020–1035.
29. Morgan JR, et al. (2013) A role for an Hsp70 nucleotide exchange factor in the regulation of synaptic vesicle endocytosis. *J Neurosci* 33:8009–8021.
30. Sousa R, Lafer EM (2015) The role of molecular chaperones in clathrin mediated vesicular trafficking. *Front Mol Biosci* 2:26.
31. Tsai CL, et al. (2018) Stress-induced phosphoprotein 1 acts as a scaffold protein for glycogen synthase kinase-3 beta-mediated phosphorylation of lysine-specific demethylase 1. *Oncogenesis* 7:31.
32. Song Y, Masison DC (2005) Independent regulation of Hsp70 and Hsp90 chaperones by Hsp70/Hsp90-organizing protein Sti1 (Hop1). *J Biol Chem* 280:34178–34185.
33. Lotz GP, Brychzy A, Heinz S, Obermann WM (2008) A novel HSP90 chaperone complex regulates intracellular vesicle transport. *J Cell Sci* 121:717–723.
34. Chen CY, Balch WE (2006) The Hsp90 chaperone complex regulates GDI-dependent Rab recycling. *Mol Biol Cell* 17:3494–3507.
35. Pavel M, et al. (2016) CCT complex restricts neuropathogenic protein aggregation via autophagy. *Nat Commun* 7:13821.
36. Bamji SX, et al. (2003) Role of beta-catenin in synaptic vesicle localization and presynaptic assembly. *Neuron* 40:719–731.
37. Brigidi GS, Bamji SX (2011) Cadherin-catenin adhesion complexes at the synapse. *Curr Opin Neurobiol* 21:208–214.
38. Arikkath J, Reichardt LF (2008) Cadherins and catenins at synapses: Roles in synaptogenesis and synaptic plasticity. *Trends Neurosci* 31:487–494.
39. Wu Y, et al. (2017) Contacts between the endoplasmic reticulum and other membranes in neurons. *Proc Natl Acad Sci USA* 114:E4859–E4867.
40. de Juan-Sanz J, et al. (2017) Axonal endoplasmic reticulum Ca^{2+} content controls release probability in CNS nerve terminals. *Neuron* 93:867–881.e6.
41. Takamori S, et al. (2006) Molecular anatomy of a trafficking organelle. *Cell* 127: 831–846.
42. Zala D, et al. (2013) Vesicular glycolysis provides on-board energy for fast axonal transport. *Cell* 152:479–491.
43. Hinckelmann MV, et al. (2016) Self-propelling vesicles define glycolysis as the minimal energy machinery for neuronal transport. *Nat Commun* 7:13233.
44. Jang S, et al. (2016) Glycolytic enzymes localize to synapses under energy stress to support synaptic function. *Neuron* 90:278–291.
45. Rangaraju V, Calloway N, Ryan TA (2014) Activity-driven local ATP synthesis is required for synaptic function. *Cell* 156:825–835.
46. Atwood BK, Lovinger DM, Mathur BN (2014) Presynaptic long-term depression mediated by Gi/o-coupled receptors. *Trends Neurosci* 37:663–673.
47. Johnson KA, Lovinger DM (2016) Presynaptic G protein-coupled receptors: Gatekeepers of addiction? *Front Cell Neurosci* 10:264.
48. Palande K, et al. (2011) Peroxiredoxin-controlled G-CSF signalling at the endoplasmic reticulum-early endosome interface. *J Cell Sci* 124:3695–3705.
49. Ryder PV, et al. (2013) The WASH complex, an endosomal Arp2/3 activator, interacts with the Hermansky-Pudlak syndrome complex BLOC-1 and its cargo phosphatidylinositol-4-kinase type IIα. *Mol Biol Cell* 24:2269–2284.
50. Speese SD, Trotta N, Rodesch CK, Aravamudan B, Broadie K (2003) The ubiquitin proteasome system acutely regulates presynaptic protein turnover and synaptic efficacy. *Curr Biol* 13:899–910.
51. Wentzel C, Delvendahl I, Sydlik S, Georgiev O, Müller M (2018) Dysbindin links presynaptic proteasome function to homeostatic recruitment of low release probability vesicles. *Nat Commun* 9:267.
52. Haas KF, Broadie K (2008) Roles of ubiquitination at the synapse. *Biochim Biophys Acta* 1779:495–506.
53. Berg D, Holzmann C, Riess O (2003) 14-3-3 proteins in the nervous system. *Nat Rev Neurosci* 4:752–762.
54. Nicholson-Fish JC, Cousin MA, Smillie KJ (2016) Phosphatidylinositol 3-kinase couples localised calcium influx to activation of Akt in central nerve terminals. *Neurochem Res* 41:534–543.
55. Ruiz A, Campanac E, Scott RS, Rusakov DA, Kullmann DM (2010) Presynaptic $GABA_A$ receptors enhance transmission and LTP induction at hippocampal mossy fiber synapses. *Nat Neurosci* 13:431–438.
56. Kullmann DM, et al. (2005) Presynaptic, extrasynaptic and axonal $GABA_A$ receptors in the CNS: Where and why? *Prog Biophys Mol Biol* 87:33–46.
57. Swanwick CC, Shapiro ME, Vicini S, Wenthold RJ (2010) Flotillin-1 promotes formation of glutamatergic synapses in hippocampal neurons. *Dev Neurobiol* 70:875–883.
58. Glebov OO, Bright NA, Nichols BJ (2006) Flotillin-1 defines a clathrin-independent endocytic pathway in mammalian cells. *Nat Cell Biol* 8:46–54.
59. Bodin S, Planchon D, Rios Morris E, Comunale F, Gauthier-Rouvière C (2014) Flotillins in intercellular adhesion—From cellular physiology to human diseases. *J Cell Sci* 127: 5139–5147.
60. Cheung G, Cousin MA (2012) Adaptor protein complexes 1 and 3 are essential for generation of synaptic vesicles from activity-dependent bulk endosomes. *J Neurosci* 32:6014–6023.
61. Gordon SL, Leube RE, Cousin MA (2011) Synaptophysin is required for synaptobrevin retrieval during synaptic vesicle endocytosis. *J Neurosci* 31:14032–14036.
62. Lyles V, Zhao Y, Martin KC (2006) Synapse formation and mRNA localization in cultured *Aplysia* neurons. *Neuron* 49:349–356.
63. Pavlos NJ, et al. (2010) Quantitative analysis of synaptic vesicle Rabs uncovers distinct yet overlapping roles for Rab3a and Rab27b in Ca^{2+}-triggered exocytosis. *J Neurosci* 30:13441–13453.
64. Nicholson-Fish JC, Smillie KJ, Cousin MA (2016) Monitoring activity-dependent bulk endocytosis with the genetically-encoded reporter VAMP4-pHluorin. *J Neurosci Methods* 266:1–10.
65. Raingo J, et al. (2012) VAMP4 directs synaptic vesicles to a pool that selectively maintains asynchronous neurotransmission. *Nat Neurosci* 15:738–745.
66. Morton A, Marland JR, Cousin MA (2015) Synaptic vesicle exocytosis and increased cytosolic calcium are both necessary but not sufficient for activity-dependent bulk endocytosis. *J Neurochem* 134:405–415.
67. Kavalali ET, Jorgensen EM (2014) Visualizing presynaptic function. *Nat Neurosci* 17: 10–16.
68. Atluri PP, Ryan TA (2006) The kinetics of synaptic vesicle reacidification at hippocampal nerve terminals. *J Neurosci* 26:2313–2320.
69. Egashira Y, Takase M, Takamori S (2015) Monitoring of vacuolar-type H^+ ATPase-mediated proton influx into synaptic vesicles. *J Neurosci* 35:3701–3710.
70. Burgoyne RD, Cambray-Deakin MA (1988) The cellular neurobiology of neuronal development: The cerebellar granule cell. *Brain Res* 472:77–101.
71. Clayton EL, et al. (2009) The phospho-dependent dynamin-syndapin interaction triggers activity-dependent bulk endocytosis of synaptic vesicles. *J Neurosci* 29: 7706–7717.
72. Kratzke M, Candiello E, Schmidt B, Jahn O, Schu P (2015) AP-1/σ1B-dependent SV protein recycling is regulated in early endosomes and is coupled to AP-2 endocytosis. *Mol Neurobiol* 52:142–161.
73. Glyvuk N, et al. (2010) AP-1/sigma1B-adaptin mediates endosomal synaptic vesicle recycling, learning and memory. *EMBO J* 29:1318–1330, and erratum (2010) 29:1941.
74. Li YC, Chanaday NL, Xu W, Kavalali ET (2017) Synaptotagmin-1- and synaptotagmin-7-dependent fusion mechanisms target synaptic vesicles to kinetically distinct endocytic pathways. *Neuron* 93:616–631.e3.

75. Kononenko NL, et al. (2014) Clathrin/AP-2 mediate synaptic vesicle reformation from endosome-like vacuoles but are not essential for membrane retrieval at central synapses. *Neuron* 82:981–988.
76. Wilhelm BG, et al. (2014) Composition of isolated synaptic boutons reveals the amounts of vesicle trafficking proteins. *Science* 344:1023–1028.
77. Grønborg M, et al. (2010) Quantitative comparison of glutamatergic and GABAergic synaptic vesicles unveils selectivity for few proteins including MAL2, a novel synaptic vesicle protein. *J Neurosci* 30:2–12.
78. Wenzel EM, et al. (2012) Key physiological parameters dictate triggering of activity-dependent bulk endocytosis in hippocampal synapses. *PLoS One* 7:e38188.
79. Chen X, et al. (2017) The BLOC-1 subunit pallidin facilitates activity-dependent synaptic vesicle recycling. *eNeuro* 4:ENEURO.0335-16.2017.
80. Inoshita T, et al. (2017) Vps35 in cooperation with LRRK2 regulates synaptic vesicle endocytosis through the endosomal pathway in *Drosophila*. *Hum Mol Genet* 26: 2933–2948.
81. Han M, et al. (2017) A systematic RNAi screen reveals a novel role of a spindle assembly checkpoint protein BuGZ in synaptic transmission in *C. elegans*. *Front Mol Neurosci* 10:141.
82. Campa CC, Hirsch E (2017) Rab11 and phosphoinositides: A synergy of signal transducers in the control of vesicular trafficking. *Adv Biol Regul* 63:132–139.
83. Braun A, et al. (2005) EHD proteins associate with syndapin I and II and such interactions play a crucial role in endosomal recycling. *Mol Biol Cell* 16:3642–3658.
84. Naslavsky N, Rahajeng J, Sharma M, Jovic M, Caplan S (2006) Interactions between EHD proteins and Rab11-FIP2: A role for EHD3 in early endosomal transport. *Mol Biol Cell* 17:163–177.
85. Darcy KJ, Staras K, Collinson LM, Goda Y (2006) Constitutive sharing of recycling synaptic vesicles between presynaptic boutons. *Nat Neurosci* 9:315–321.
86. Staras K, et al. (2010) A vesicle superpool spans multiple presynaptic terminals in hippocampal neurons. *Neuron* 66:37–44.
87. Delevoye C, et al. (2014) Recycling endosome tubule morphogenesis from sorting endosomes requires the kinesin motor KIF13A. *Cell Rep* 6:445–454.